

## RECONSTRUCTION AND DISPLAY OF THE RETINA

*Kenneth R. Sloan, Jr.*

*David Meyers*

Department of Computer Science, FR-35  
University of Washington  
Seattle WA 98195  
U.S.A.

*Christine A. Curcio*

Departments of Biological Structure and Ophthalmology  
University of Washington  
Seattle WA 98195  
U.S.A.

### ABSTRACT

The retina is an approximately spherical structure. In order to gather information such as the density of rods and cones it is necessary to flatten the retina. It is desirable to project these measurements back onto the original spherical form of the retina, interpolate the sampled data, and display the results. This paper is a summary of techniques which we have developed to perform these tasks.

### RÉSUMÉ

La rétine peut être approximée par une surface sphérique. Pour recueillir certaines informations comme la densité des cônes et des bâtonnets, il faut aplatir la rétine. Nous aimerions reprojeter ces mesures sur la surface sphérique originale, interpoler les données recueillies et afficher les résultats. Cet ouvrage est une synthèse des techniques que nous avons développées pour effectuer ces tâches.

**KEYWORDS:** human retina, reconstruction, spherical geometry, interpolation.

### 1. Introduction

The topography of the constituent cells and efferent pathways of the retina is important for understanding how the visual world is sampled and how it is represented in the central nervous system. The retinal whole mount is the histological method of choice for revealing these topographical relationships (Stone, 1981, for review). Because the retina covers the major part of the sphere, it must be cut so that it can be flattened for viewing under a microscope. Thus, a general problem with whole mounts is that spatial relationships are lost across the cut edges. Furthermore, locations of features on the retinal sphere, which in theory could be specified with great precision, are not readily determined from their positions in the flattened tissue.

These problems may be solved by reconstructing the original spherical surface from the flattened tissue. Such a reconstruction has been accomplished manually by approximating tracings of the tissue to the surface of a sphere of appropriate diameter (e.g., Østerberg, 1935).

The advent of sophisticated and affordable computer technology has made digital reconstruction techniques possible. We report methods for specifying a retinal coordinate system, reconstituting the retinal sphere from a three-piece whole mount (Curcio, *et al.*, in preparation), and displaying topographic data.

Our key reconstruction step relies on the fact that one of the three pieces of the retina has a particularly easy mapping back to the sphere, based on natural landmarks. Once this piece has been placed on the sphere, the other two are positioned relative to it, using a small set of fiducial points. In the first case, we can assume that there has been little or no distortion of the tissue. For the second placement problem, we cannot make this assumption. Instead, we assume that the tissue has been warped, and rely on an iterative relaxation procedure to place each point.

The reconstructed retina is then used as the basis for display. We construct a triangular mesh connecting

---

This work was supported in part by the National Science Foundation under grant number DCR - 8505713, by a Lions Northwest Training Fellowship, and by the National Institutes of Health under grant number EY04536.

the sampled points. Measured quantities (rod, cone and ganglion cell densities) are represented as intensities (usually false-colored). The triangular mesh can be directly displayed to give a direct three-dimensional view of the retina, or projected onto the plane in the style of conventional visual field maps. To generate a true visual field map, we can back-project the retina through a standard model of the eye's optics.

The display techniques have been applied to Østerberg's data (1935), and have provided invaluable guidance in the design of the sampling scheme which we are using now.

## 2. Coordinate Systems

### 2.1 Retinal Sphere

The retina is treated as the surface of a unit sphere. Any point on the sphere can be indexed by two coordinates,  $\lambda$  (longitude, meridian) and  $\phi$  (colatitude, eccentricity). This coordinate system allows us to make comparisons between eyes of different diameters.

Eccentricity is measured from the center of the fovea. The nasal horizontal ( $0^\circ$ ) meridian is defined as the meridian passing through the center of the fovea and the center of the optic disk. The superior vertical meridian is at  $90^\circ$ , temporal horizontal meridian is at  $180^\circ$ , and the inferior vertical meridian is at  $270^\circ$ .

### 2.2 Microscope stage

We developed a 3-piece whole mount dissection technique which results in a belt  $60^\circ$  wide roughly centered on the horizontal meridian, and two caps from the inferior and superior retina. These three pieces can be flattened without tearing the retina; the belt is only very slightly distorted.

The locations of data points on the whole mount are expressed in terms of the X,Y coordinates of the microscope vernier. The raw data base consists of a collection of such X,Y points, along with measurements made at these locations, such as the density of rods or cones.

In order to assist in the reconstruction, we also note the positions of the fovea, the optic disc, and several (about ten) *key points* (usually blood vessels) along each of the shared boundaries between the belt and the caps.

### 2.3 Visual field

It is important to be able to express retinal location in terms of functionally defined locations in the visual field. The projection of the visual field onto the retina has been deduced by tracing the path of rays through the optical apparatus of an average eye. The projection is nonlinear, such that a degree of visual angle subtends a greater extent of retina centrally than peripherally. The exact nature

of the nonlinearity varies among different schematic eyes, based on different underlying assumptions (*e.g.*, Drasdo and Fowler, 1974). One advantage of our decision to keep all retina data in a retina-based coordinate system is that it remains available for transformation to visual field coordinates by any suitable schematic eye.

## 3. Mappings

### 3.1 Three Planar Patches $\implies$ One

The three separate planar patches (Belt, Inferior Cap and Superior Cap) are positioned in a common, planar coordinate system so that (see Figure 1):

- the fovea is at the origin
- the optic disc is on the positive x axis
- the inferior and superior caps are attached to, and tangent to, the belt, at a common key point.

### 3.2 Plane $\implies$ Sphere

Mapping the central belt to the sphere is relatively easy. The shape and extent of this patch was chosen so that it could be flattened easily, without appreciable distortion. The fovea and optic disc provide all the landmarks necessary to orient the planar stage coordinates with respect to our spherical coordinate system. All that needs to be done is to wrap the rectangular belt around the sphere. First, we estimate the diameter of the retinal sphere by measuring the outer diameter of the eye, and the thickness of the sclera. The  $(x, y)$  coordinates can then be scaled from mm (as measured by the microscope vernier) to degrees of arclength (as measured on the unit sphere). They can then be considered to be two sides of a right spherical triangle. The  $(\lambda, \phi)$  coordinates are straightforward to calculate from this triangle.

This calculation correctly maps all points in the belt (including the belt's version of the keypoints) onto the sphere. However, it provides only a very gross estimate of the position of a point in either of the caps.

In order to position a cap point, we use an iterative relaxation process. In the planar stage coordinates, we calculate the distance between the cap point and each of the key points in that cap. After mapping to the sphere, we discard the key points associated with the cap, and look at the corresponding key points in the belt. These points have been correctly positioned on the sphere. We measure the (great circle) directions and distances between the cap point and each key point. Of course, the distances will be different than those measured in the plane. By taking the vector sum of these differences, and moving the cap point (on the sphere) until this sum approaches zero, we find a point on the sphere which minimizes our placement error. The process is observed to converge in some 10-30 iterations.

It is very important to properly weight the effect of individual key points. On the one hand, each key point provides some information about the proper placement of a particular point. On the other hand, key points which are very far away are less reliable, primarily because the warping is likely to be very non-linear over large distances.

Giving each key point equal weight results in obvious, gross errors. Weighting each key point by the inverse of the (planar) distance to the point to be placed is significantly better, but still produces an occasional misplacement. Inverse square distance is currently in use, and appears to appropriately balance the contribution of each key point to the final placement.

After this mapping, we have the original data points positioned in our canonical spherical coordinate system. See Figure 2.

#### 4. Triangulation

Effective display of this data requires more than isolated data points. We would like to fit a surface to these points, and use that surface to provide estimates of the measured quantities everywhere on the retina. A first step in this direction is to tessellate the sphere with triangular patches, using the data points as vertices.

The data points are connected into a triangular net by projecting them back into the plane and computing local equiangular triangulation of the projected points, which is the completion of the Delaunay tessellation (Sibson, 1978). Given the relatively small size of our data (typically 200 points), we directly calculate the equiangular triangulation.

The projection to the plane used is the equidistant (polar azimuthal equidistant) projection (Frisen, 1970) - achieved by treating the spherical  $(\lambda, \phi)$  coordinates as *polar* coordinates. This projection preserves radial distances (eccentricity), while stretching tangential distances. The surface of the sphere maps into a disc of radius  $\pi$ . The worst distortion is at the opposite pole, which maps to the circle surrounding this disc.

In the plane, the Delaunay triangulation is optimal in the sense that the triangles are as compact as possible. When projected back to the sphere, this triangulation is very good near the fovea, and less so near the periphery.

#### 5. Display

The last problem is to display this spherical triangular mesh, with measured density values at each vertex. The customary method of presenting visual field data is to project to the plane (using the equidistant projection) and plot the density values as gray levels (or isodensity contours). It is easy to augment this display with gamma correction and false coloring (Sloan and Brown, 1979). We have a choice of painting each triangle with an average intensity value, or of interpolating the values measured at the vertices (see Figures 3-7). In either case, the triangulation developed above is exactly right for this projection.

This display is similar to those that anatomists and ophthalmologists are used to seeing, and have little trouble interpreting. We can also, of course, display the triangular mesh (colored as above) as a three dimensional, spherical surface. Going further, we can use the measured densities to deform the surface away from the sphere. Finally, we are beginning work on fitting a smooth surface to the data, using our triangular mesh as a control graph. The methods of (Farin, 1983) can be applied directly to our data.

#### 6. Discussion

Østerberg's paper (1935) on the distribution of rods and cones in the human eye is one of the most widely cited studies in the vision literature. The findings most frequently cited and reprinted are the density of rods and cones along the horizontal meridian and the calculation of the total number of photoreceptors. His data on the overall topography of photoreceptors, illustrated by density maps (contours for rods, symbols for cones) are less well appreciated, mainly because of the relatively less accessible nature of his maps. Our display techniques, applied to this data, provide much better intuition about the gross topography, and have pointed out deficiencies in his sampling scheme.

For example, look at Figure 6, which shows the central  $8^\circ$  of Østerberg's eye. Notice that he sampled very finely along the  $0^\circ$  meridian, but much more coarsely in other directions. When this sampling is displayed directly, it gives a distorted picture of the shape of the density map. If one assumes that the map is radially symmetric, then a better-looking density map could be constructed (by duplicating the  $0^\circ$  points), but this "better-looking" picture would be more a product of the assumption than of the measured data. By comparison, look at Figure 7, which shows the same central  $8^\circ$  of a more recent eye.

### 7. References

1. Curcio, C.A., D. Meyers, and K.R. Sloan, Jr. (in preparation) computer methods for reconstruction, display, and analysis of whole mounts: applications to human photoreceptor topography.
2. Drasdo, N. and C.W. Fowler (1974) Non-linear projection of the retinal maps in a wide-angle schematic eye. *Br. J. Ophthalmol.* 47: 609-613.
3. Farin, G. (1983) Smooth Interpolation to Scattered 3D Data. in *Surfaces in CAGD*, ed. Robert E. Barhill and Wolfgang Böhm, North-Holland Publishing Company, Amsterdam, pp. 43-63.
4. Frisen, L. (1970) The cartographic deformations of the visual field. *Ophthalmologica* 161:38-54.
5. Graham, R. L. (1972) An Efficient Algorithm For Determining The Convex Hull Of A Finite Planar Set. *Information Processing Letters* 1: pp. 132-133.
6. Østerberg, G.A. (1935) Topography of the layer of rods and cones in the human retina. *Acta Ophthalmol* 13 Suppl. 5 pp. 1-102.
7. Sibson, R. (1978) Locally Equiangular Triangulation. *The Computer Journal* 21:3 pp. 243-245.
8. Stone, J. (1981) *The whole mount handbook*. Sydney: Maitland.
9. Sloan, K.R. and C.M. Brown (1979) Color map techniques. *CG&IP* 10, 296-316.

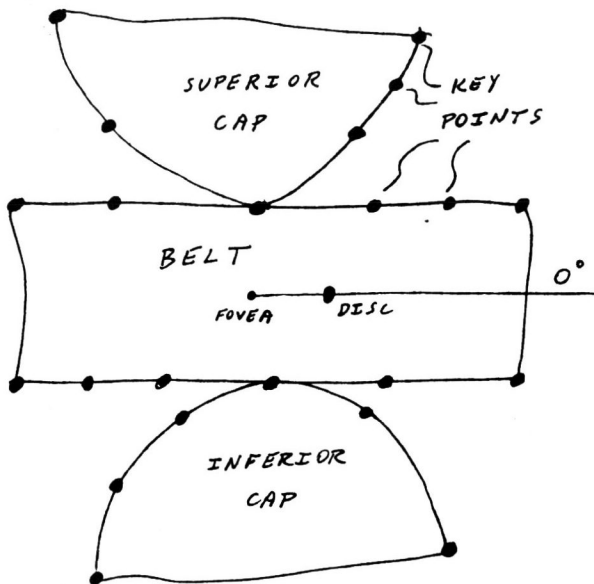


Figure 1. the three-piece dissection. The belt is roughly rectangular, and can be positioned on the sphere using the fovea and optic disc as landmarks. The inferior (superior) cap is positioned relative to the belt by means of key points which can be located in both the belt and the cap.



and cute TeX hacks, such as these silly pictures.

**Kenneth R. Sloan, Jr.** was born in Millington, TN, on June 12, 1947. He received a Ph.D. in Computer and Information Science from the University of Pennsylvania. His research interests include graphics, (computer) vision, artificial intelligence, distributed computing, and cute TeX hacks, such as these silly pictures.



while skiing, he works as a Research Technologist at the University of Washington, where he is also studying Computer Science.

**David Meyers** was born July 8, 1949. He attended the University of Colorado where he received his B.S. in Cell Biology. He came to Seattle in 1975. While not hanging from the end of a trapeze wire on a 505 class dinghy, or attempting to bury himself headfirst in a snowbank



and knows what the pictures really mean.

**Christine A. Curcio** was born on November 16, 1950 and received a Ph.D. in Anatomy from the University of Rochester. She is interested in the organization of the retina, aging of the nervous system, and computer-assisted morphometry. She counted the rods and cones,

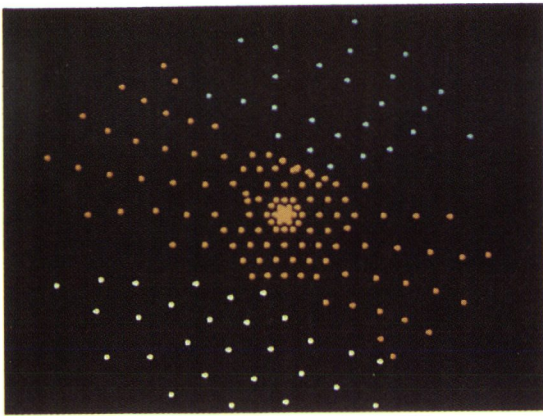


Figure 2. Sample points from a typical reconstruction, displayed using the polar azimuthal equidistant projection.

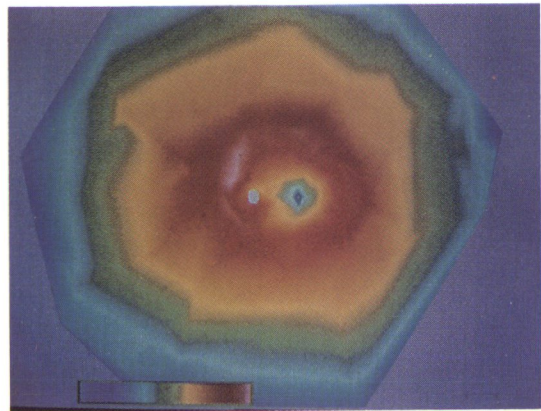


Figure 3. A display of Østerberg's rod density data, smooth shaded (in the plane) and false colored.

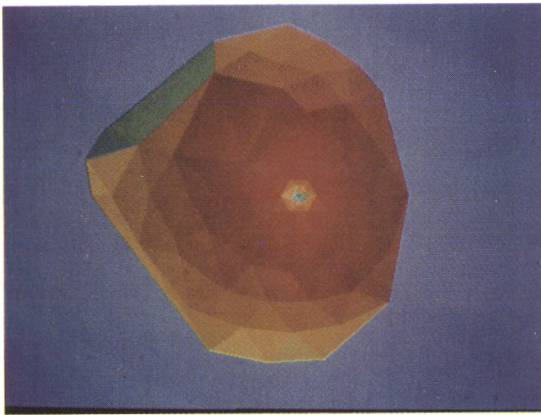


Figure 4. A rod map from a different eye, with the triangles shaded according to the average density at each vertex.

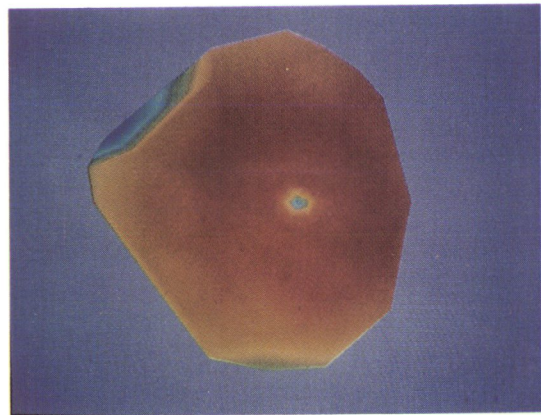


Figure 5. The same rod map as in Figure 4, displayed smooth shaded.

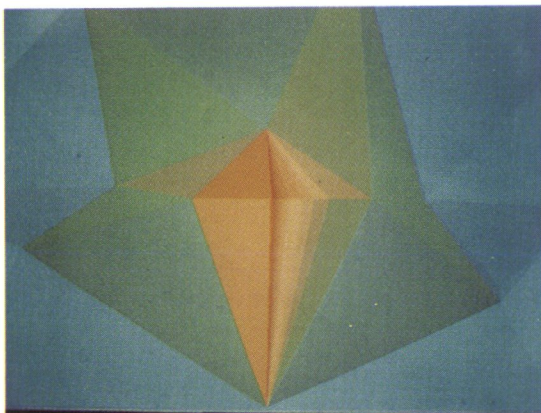


Figure 6. The central 8° of Østerberg's cone density data. Note the anisotropic sampling, and the "kite-shaped" pattern.

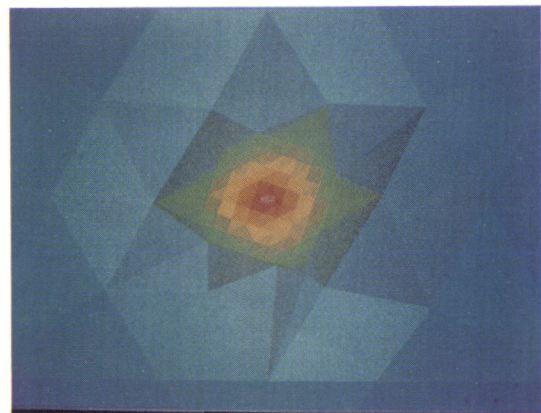


Figure 7. The central 8° of one of our recent eyes.